Salomäki, J., Piippo, A., Hinkkanen, M., and Luomi, J. (2006). Sensorless vector control of PMSM drives equipped with inverter output filter. In Proceedings of the 32nd Annual Conference of the IEEE Industrial Electronics Society (IECON 2006), Paris, France, pp. 1059-1064.

Sensorless Vector Control of PMSM Drives Equipped With Inverter Output Filter

Janne Salomäki, Antti Piippo, Marko Hinkkanen, and Jorma Luomi

Power Electronics Laboratory
Helsinki University of Technology
P.O. Box 3000, FI-02015 TKK, Finland
janne.salomaki@tkk.fi

***Abstract*— The paper presents a sensorless vector control method for a permanent magnet synchronous motor when the output voltage of the PWM inverter is filtered by an LC filter. The dynamics of the LC filter are taken into account in the design of the controller and adaptive full-order observer. The use of the output filter does not require additional current or voltage measurements. The speed adaptation is based on the estimation error of the inverter output current. Linearization analysis is used to design an observer that enables a wide operation region. Simulation and experimental results show the functionality of the proposed control method.**

I. Introduction

Problems may be encountered in AC motor drives due to the non-sinusoidal voltage produced by a pulse-width modulated (PWM) inverter. The high rate of change of the voltage (i.e. high $\mathrm{d}u/\mathrm{d}t$) may cause excessive voltage stresses in the stator winding insulations. It may also cause leakage currents through the parasitic capacitances of the stator winding and produce bearing currents. Lower-order harmonics cause acoustic noise and power losses; the losses caused by eddy currents are a special concern in high-speed solid-rotor motors.

A common approach to overcome these problems is to use an inverter output filter [1]–[6]. An LC filter, having the resonance frequency below the switching frequency, is a typical choice for the filter topology if a nearly sinusoidal output voltage is required. However, this kind of heavy filtering affects the vector control of the motor. The filter dynamics should be taken into account in the control design.

Various methods have been proposed for the vector control of variable-speed drives equipped with an LC filter. Methods based on a feedforward action and sliding mode control have been proposed for compensating the effects of the filter in a sensorless permanent magnet synchronous motor (PMSM) drive [4]. A model-based observer and an adaptive speed estimator have been implemented in the stator reference frame for estimating the rotor angle and speed in a sensorless PMSM drive [5]. A feedforward current controller has been used in a speed-sensored synchronous reluctance motor drive with an LC filter [6]. In these methods, stator current or stator voltage measurements are needed. Vector control methods for induction motor drives with an LC filter in [7]–[12] also require measurements from the motor side of the filter.

If the control method requires only the measurements of the inverter output current and the dc-link voltage, a filter can be added to an existing drive, and no hardware modifications are needed in the frequency converter. Full-order observers have recently been proposed for induction motor drives equipped with an LC filter [13]–[15], thus avoiding additional current or voltage measurements.

In this paper, a sensorless control method is developed for a PMSM drive equipped with an LC filter. Cascaded controllers are used for controlling the inverter current, the stator voltage, and the stator current. An adaptive full-order observer is used for estimating the stator voltage, the stator current, the rotor speed, and the rotor position. The observer gain is selected by using a linearized model. Finally, simulation and experimental results are presented.

II. Filter and Motor Models

Fig. 1 shows a PMSM drive system equipped with an LC filter. The inverter output voltage $\mathbf{u}_A$ is filtered by the LC filter, resulting in a nearly sinusoidal stator voltage $\mathbf{u}_s$. The inverter output current $\mathbf{i}_A$ and the dc-link voltage u_{dc} are the only measured quantities.

In the d-q reference frame fixed to the rotor, the model of the three-phase LC filter and the PMSM can be written as

$$\dot{\mathbf{x}} = \mathbf{A}\mathbf{x} + \mathbf{B}\begin{bmatrix}\mathbf{u}_A & \boldsymbol{\psi}_{pm}\end{bmatrix}^T \tag{1}$$

$$\mathbf{i}_A = \mathbf{C}\mathbf{x} \tag{2}$$

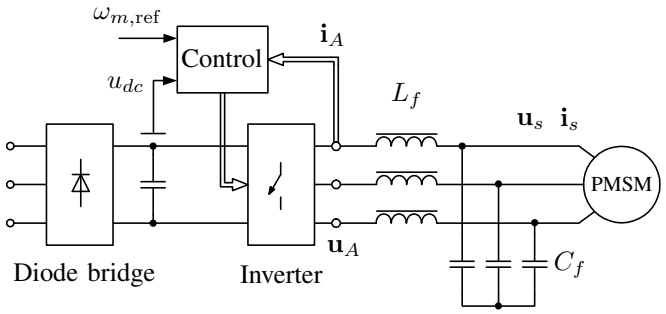

Fig. 1. PMSM drive system equipped with three-phase LC filter.

where $\mathbf{x} = \begin{bmatrix}\mathbf{i}_A & \mathbf{u}_s & \boldsymbol{\psi}_s\end{bmatrix}^T$ is the state vector consisting of the inverter output current $\mathbf{i}_A = \begin{bmatrix}i_{Ad} & i_{Aq}\end{bmatrix}^T$, the stator voltage $\mathbf{u}_s = \begin{bmatrix}u_{sd} & u_{sq}\end{bmatrix}^T$, and the stator flux linkage $\boldsymbol{\psi}_s = \begin{bmatrix}\psi_{sd} & \psi_{sq}\end{bmatrix}^T$. The inverter output voltage $\mathbf{u}_A = \begin{bmatrix}u_{Ad} & u_{Aq}\end{bmatrix}^T$ and the permanent magnet flux $\boldsymbol{\psi}_{pm} = \begin{bmatrix}\psi_{pm} & 0\end{bmatrix}^T$ are considered as inputs to the system. The matrix transpose is denoted by superscript T. The system matrices in (1) and (2) are

$$\mathbf{A} = \begin{bmatrix} -R_{Lf}L_f^{-1}\mathbf{I} - \omega_m\mathbf{J} & -L_f^{-1}\mathbf{I} & \mathbf{0} \\ C_f^{-1}\mathbf{I} & -\omega_m\mathbf{J} & -C_f^{-1}\mathbf{L}_s^{-1} \\ \mathbf{0} & \mathbf{I} & -R_s\mathbf{L}_s^{-1} - \omega_m\mathbf{J} \end{bmatrix} \tag{3}$$

$$\mathbf{B} = \begin{bmatrix} L_f^{-1}\mathbf{I} & \mathbf{0} \\ \mathbf{0} & C_f^{-1}\mathbf{L}_s^{-1} \\ \mathbf{0} & R_s\mathbf{L}_s^{-1} \end{bmatrix} \tag{4}$$

$$\mathbf{C} = \begin{bmatrix}\mathbf{I} & \mathbf{0} & \mathbf{0}\end{bmatrix} \tag{5}$$

where L_f is the inductance and R_{Lf} is the series resistance of the filter inductor, C_f is the filter capacitance, R_s is the stator resistance, ω_m is the electrical angular speed of the rotor, and

$$\mathbf{I} = \begin{bmatrix}1 & 0\\ 0 & 1\end{bmatrix}, \quad \mathbf{J} = \begin{bmatrix}0 & -1\\ 1 & 0\end{bmatrix}$$

The stator inductance matrix

$$\mathbf{L}_s = \begin{bmatrix}L_d & 0\\ 0 & L_q\end{bmatrix}$$

consists of the direct-axis inductance L_d and quadrature-axis inductance L_q.

III. Control System

Fig. 2 shows a simplified block diagram of the control system (the estimated quantities being marked by $\hat{}$). The cascade control and the speed-adaptive full-order observer are implemented in the estimated rotor reference frame. The estimated rotor position $\hat{\theta}_m$ is obtained by integrating $\hat{\omega}_m$.

The inverter current, the stator voltage, and the stator current are controlled by PI controllers, and cross-couplings due to the rotating reference frame are compensated. A simple one-step-ahead current prediction is used in the inverter current control in a fashion similar to [16]. A maximum torque per current method [17] is used for calculating the stator current reference. The rotor speed is governed by a PI controller with active damping.

IV. Speed-Adaptive Full-Order Observer

A. Observer Structure

A speed-adaptive full-order observer has been successfully used in a sensorless induction motor drive equipped with an LC filter [14], [15]. A similar observer structure is constructed for the PMSM drive in the following.

The inverter current is the feedback signal for the observer, and the electrical angular speed of the rotor is estimated using an adaptation mechanism. The observer is defined by

$$\dot{\hat{\mathbf{x}}} = \hat{\mathbf{A}}\,\hat{\mathbf{x}} + \mathbf{B}\begin{bmatrix}\mathbf{u}_A & \hat{\boldsymbol{\psi}}_{pm}\end{bmatrix}^T + \mathbf{K}(\mathbf{i}_A - \hat{\mathbf{i}}_A) \tag{6}$$

where the system matrix and the observer gain matrix are

$$\hat{\mathbf{A}} = \begin{bmatrix} -R_{Lf}L_f^{-1}\mathbf{I} - \hat{\omega}_m\mathbf{J} & -L_f^{-1}\mathbf{I} & \mathbf{0} \\ C_f^{-1}\mathbf{I} & -\hat{\omega}_m\mathbf{J} & -C_f^{-1}\mathbf{L}_s^{-1} \\ \mathbf{0} & \mathbf{I} & -R_s\mathbf{L}_s^{-1} - \hat{\omega}_m\mathbf{J} \end{bmatrix} \tag{7}$$

$$\mathbf{K} = \begin{bmatrix} k_{1d}\mathbf{I} + k_{1q}\mathbf{J} \\ k_{2d}\mathbf{I} + k_{2q}\mathbf{J} \\ k_{3d}\mathbf{I} + k_{3q}\mathbf{J} \end{bmatrix}, \tag{8}$$

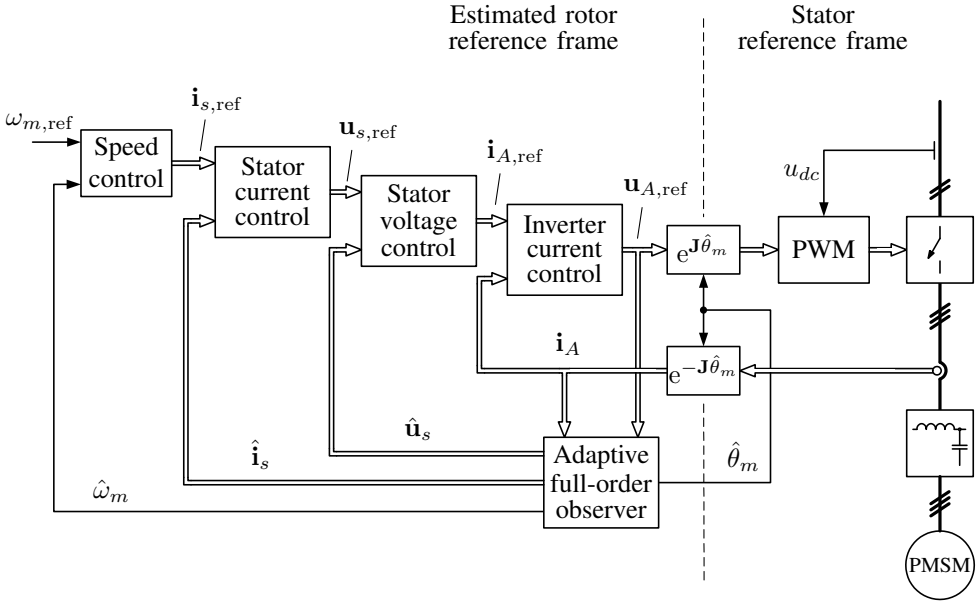

Fig. 2. Simplified block diagram of the control system. Double lines indicate vector quantities whereas single lines indicate scalar quantities. The speed control includes the calculation of the stator current reference according to the maximum torque per current method.

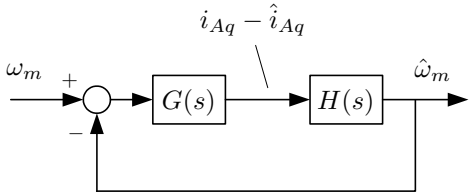

Fig. 3. Signal flow diagram of linearized model.

respectively. The factors k_{id} and k_{iq} ($i = 1,\ 2,\ 3$) are scalar gain parameters. The adaptation law is

$$\hat{\omega}_m = -K_p\,(i_{Aq} - \hat{i}_{Aq}) - K_i \int (i_{Aq} - \hat{i}_{Aq})dt \qquad (9)$$

where K_p and K_i are nonnegative adaptation gains. The digital implementation of the adaptive full-order observer is based on a symmetric Euler method [18].

B. Linearization

Adaptive observers can be analysed via linearization [19], [20]. The following linearization is carried out in the estimated rotor reference frame in a fashion similar to [21]. Accurate parameter estimates are assumed for the analysis. The estimation error of the rotor position $\tilde{\theta}_m = \theta_m - \hat{\theta}_m$ is taken into account in the system equation (1), and operating-point quantities are marked by the subscript 0. The resulting linearized model is

$$\begin{bmatrix} \dot{\tilde{\mathbf{x}}} \\ \dot{\tilde{\theta}}_m \end{bmatrix} = \underbrace{\begin{bmatrix} \mathbf{A}_0 - \mathbf{K}_0\mathbf{C} & \mathbf{D}_0 \\ \mathbf{0} & 0 \end{bmatrix}}_{\mathbf{A}'} \begin{bmatrix} \tilde{\mathbf{x}} \\ \tilde{\theta}_m \end{bmatrix} + \underbrace{\begin{bmatrix} \mathbf{0} \\ 1 \end{bmatrix}}_{\mathbf{B}'} \tilde{\omega}_m \qquad (10)$$

where

$$\mathbf{D}_0 = \begin{bmatrix} 0 \\ 0 \\ C_f^{-1}\mathbf{J}\mathbf{L}_s^{-1}(\boldsymbol{\psi}_{pm} - \boldsymbol{\psi}_{s0}) + C_f^{-1}\mathbf{L}_s^{-1}\mathbf{J}\boldsymbol{\psi}_{s0} \\ R_s\mathbf{J}\mathbf{L}_s^{-1}(\boldsymbol{\psi}_{pm} - \boldsymbol{\psi}_{s0}) + R_s\mathbf{L}_s^{-1}\mathbf{J}\boldsymbol{\psi}_{s0} \end{bmatrix} \qquad (11)$$

TABLE I

Motor Parameters	
Stator resistance R_s	3.59 Ω
Direct-axis inductance L_d	36.0 mH
Quadrature-axis inductance L_q	51.0 mH
Permanent magnet flux ψ_{pm}	0.545 Vs
Total moment of inertia J	0.015 kgm^2
Rated speed	1500 r/min
Rated current (rms)	4.3 A
Rated torque	14.0 Nm
LC Filter Parameters	
Inductance L_f	5.1 mH
Capacitance C_f	6.8 μF
Series resistance R_{Lf}	0.1 Ω

The transfer function from the rotor speed estimation error $\tilde{\omega}_m = \omega_m - \hat{\omega}_m$ to the q component of the inverter current estimation error $\tilde{i}_{Aq} = i_{Aq} - \hat{i}_{Aq}$ is

$$G(s) = \mathbf{C}'(s\mathbf{I} - \mathbf{A}')^{-1}\mathbf{B}' \qquad (12)$$

where $\mathbf{C}' = \begin{bmatrix} 0 & 1 & 0 & 0 & 0 & 0 & 0 \end{bmatrix}$. Based on (9), the transfer function from $i_{Aq} - \hat{i}_{Aq}$ to the rotor speed estimate $\hat{\omega}_m$ is

$$H(s) = -K_p - \frac{K_i}{s}. \qquad (13)$$

The resulting linearized model is illustrated in Fig. 3.

C. Observer Gain Selection

The linearized model is used for the observer gain selection. The parameters of a 2.2-kW six-pole interior-magnet PMSM (370 V, 75 Hz) and an LC filter, used for the following analysis, are given in Table I. The base values of the angular frequency, current, and voltage are $2\pi \cdot 75$ rad/s, $\sqrt{2} \cdot 4.3$ A, and $\sqrt{2/3} \cdot 370$ V, respectively. The parameter values $K_p = 25\ (\mathrm{As})^{-1}$ and $K_i = 20\,000\ (\mathrm{As}^2)^{-1}$ are used in the speed adaptation.

Fig. 4(a) shows the poles of the linearized model as the observer gain is zero, i.e. $\mathbf{K} = [\mathbf{0}\ \mathbf{0}\ \mathbf{0}]^T$. The angular speed of the rotor varies from -1 p.u. to 1 p.u. and the load torque

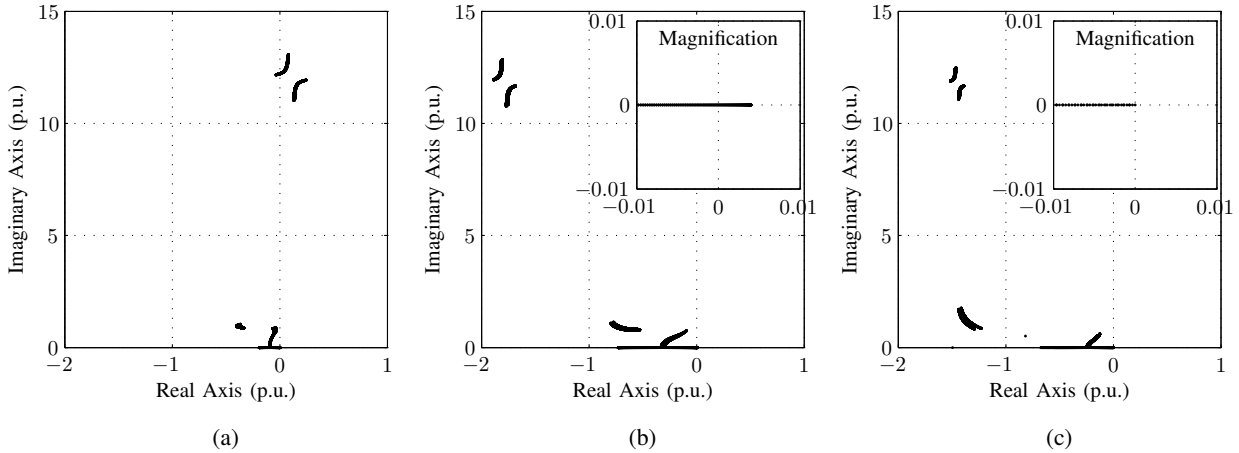

Fig. 4. Poles of linearized model as rotor angular speed ω_{m0} is varied from -1 p.u. to 1 p.u. and load torque is at positive rated value. Observer gain is (a) $\mathbf{K} = [\mathbf{0}\ \mathbf{0}\ \mathbf{0}]^T$, (b) $\mathbf{K} = [(2000\ \mathrm{s}^{-1})\mathbf{I}\ \mathbf{0}\ \mathbf{0}]^T$, and (c) proposed gain.

is at the positive rated value. The adaptive observer is unstable because of poles in the right half-plane. Due to the presence of the LC filter, zero gain cannot be used in the observer. Similar behavior has been reported for induction motor drives [13]–[15].

The instability caused by the LC filter can be avoided by using a simple constant gain:

$$\mathbf{K} = \begin{bmatrix} k_{1d}\mathbf{I} & \mathbf{0} & \mathbf{0} \end{bmatrix}^T \tag{14}$$

Fig. 4(b) shows the poles obtained using (14) with $k_{1d} = 2000\ \mathrm{s}^{-1}$. The poles originating from the LC filter are moved to the left half-plane. However, the saliency of the PMSM still causes instability at low speeds in the motoring mode [21]. In this example, right half-plane poles appear at the rated load in the speed range between 0 and 0.08 p.u.

To further improve the stability, the gain

$$\mathbf{K} = \begin{bmatrix} k_{1d}\mathbf{I} \\ \mathbf{0} \\ k_{3d}\mathbf{I} + k_{3q}\mathrm{sign}(\hat{\omega}_m)\mathbf{J} \end{bmatrix} \tag{15}$$

is proposed. Fig. 4(c) shows the poles obtained using this gain with $k_{1d} = 2000\ \mathrm{s}^{-1}$ and $k_{3d} = k_{3q} = 4R_s$. All poles stay in the left half-plane in the whole inspected operation region (except a pole in the origin at $\omega_m = 0$). It is to be noted that in practice, parameter and measurement errors cause stability problems at low speeds under load.

V. Simulation Results

The system was investigated by computer simulations using the MATLAB/Simulink software. Accurate motor and filter parameters, given in Table I, were used in the control. The sampling frequency was equal to the switching frequency of 5 kHz. The bandwidths of the controllers were $2\pi \cdot 600$ rad/s for the inverter current, $2\pi \cdot 400$ rad/s for the stator voltage, $2\pi \cdot 200$ rad/s for the stator current, and $2\pi \cdot 4$ rad/s for the rotor speed.

Fig. 5 shows a simulated comparison of the observer gains (14) and (15). The speed reference is kept constant, and rated load torque is applied stepwise at $t = 0.5$ s. In Fig. 5(a), the constant gain (14) is used, and the system becomes unstable after the load torque step. Fig. 5(b) shows the same sequence using the proposed gain (15). The system works now successfully.

Fig. 6 shows simulation results obtained for a sequence consisting of a speed reference step from zero speed to 0.67 p.u., a rated load torque step, a load removal, and a deceleration to standstill. The proposed observer and control method work fine. It is to be noted that the q components of the inverter and stator currents are nearly equal in steady state, but the d components differ from each other at higher speeds. After the deceleration, a steady-state error exists in the rotor position estimation because the system is not observable at standstill.

VI. Experimental Results

The experimental setup is illustrated in Fig. 7. The frequency converter was controlled by a dSPACE DS1103 PPC/DSP board. The motor and filter data are given in Table I. At the startup, a dc voltage was applied for 0.4 s to force-align the rotor with the stator-produced magnetic field before the controllers and the observer were enabled. Simple current feedforward compensation for dead times and power device voltage drops was applied [22].

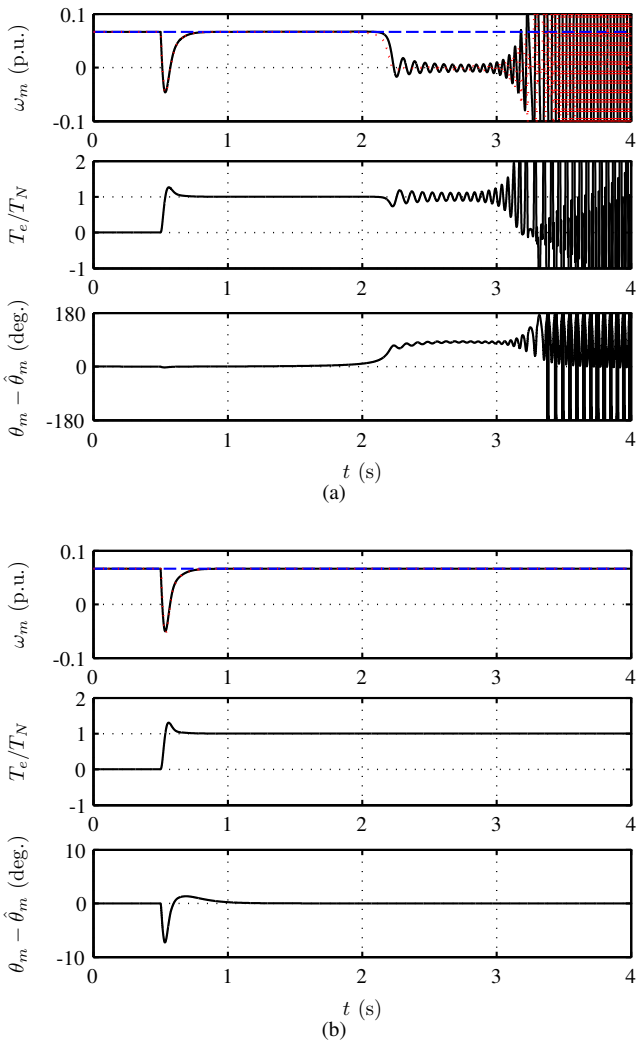

Fig. 5. Simulation results showing rated load torque step using (a) constant observer gain (14) and (b) proposed observer gain (15). Speed reference is set to 0.067 p.u. (5 Hz). The first subplot shows the speed reference (dashed), the actual rotor speed (solid), and its estimate (dotted). The second subplot shows the electromagnetic torque of the PMSM. The third subplot shows the estimation error of the rotor position in electrical degrees.

Fig. 8 shows experimental results corresponding to the simulation shown in Fig. 6. The measured performance is in accordance with the simulation results. An oscillation at the sixth harmonic can be seen in the currents under load. This oscillation originates mainly from the inductance harmonics of the motor; it exists even when the drive is used without the filter.

Fig. 9 shows experimental results obtained for a sequence consisting of an acceleration to 0.27 p.u., a rated load torque step, a speed reversal, a load removal, and a deceleration to standstill. The fast speed reversal is successful. The inverter and stator voltage and current waveforms are shown in detail in

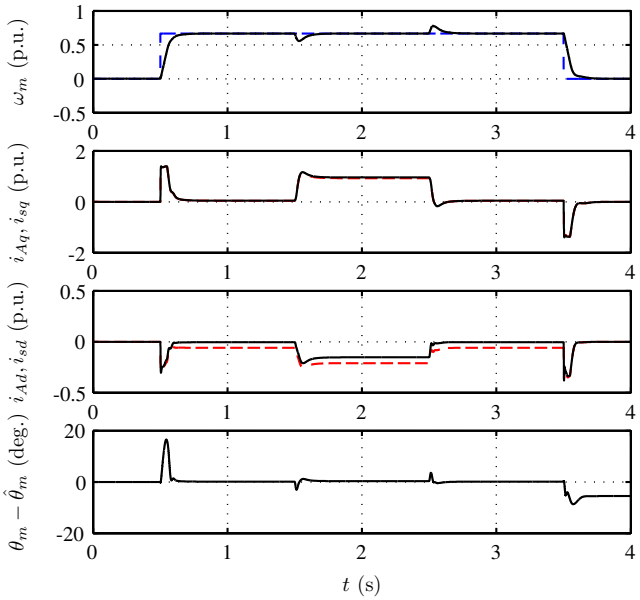

Fig. 6. Simulation results showing a sequence with speed and load changes. The first subplot shows the speed reference (dashed), the actual rotor speed (solid), and its estimate (dotted). The second subplot shows the q components of the stator (solid) and inverter (dashed) currents. The third subplot shows the d components of the stator (solid) and inverter (dashed) currents. The fourth subplot shows the estimation error of the rotor position in electrical degrees.

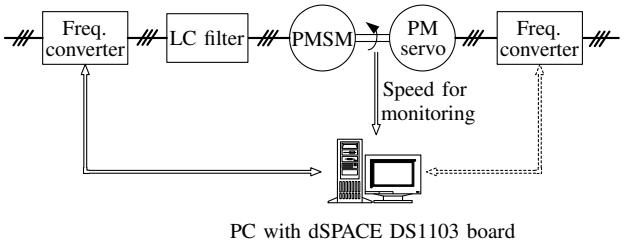

PC with dSPACE DS1103 board

Fig. 7. Experimental setup. The permanent magnet (PM) servo motor is used as the loading machine.

Fig. 10. The stator voltage and current are close to sinusoidal.

Fig. 11 shows experimental speed-torque curves as the speed reference is kept constant and the load torque is slowly changed from rated torque to negative rated torque. The duration of each torque reversal was 60 seconds. The figure illustrates the operation range of the drive. The control works fine at high speeds. At low speeds, the inverter output voltage is close to zero and the nonidealities of the inverter deteriorate the performance. When the speed is 0.025 p.u. (2 Hz), operation in the regeneration mode is not possible, but the drive withstands loads up to the rated torque in the motoring mode.

VII. Conclusion

Nested control loops and an adaptive full-order observer can be used for the sensorless vector control of a PMSM drive equipped with an LC filter at the inverter output. Only the inverter output current and the dc-link voltage need to be measured. Hence, it is possible to add a filter to an existing drive without any hardware modifications in the frequency converter. Linearization analysis is a suitable method for designing an observer gain for the system. Simulation and experimental results show that the performance of the proposed control method is good, comparable to that of the drive without the filter.

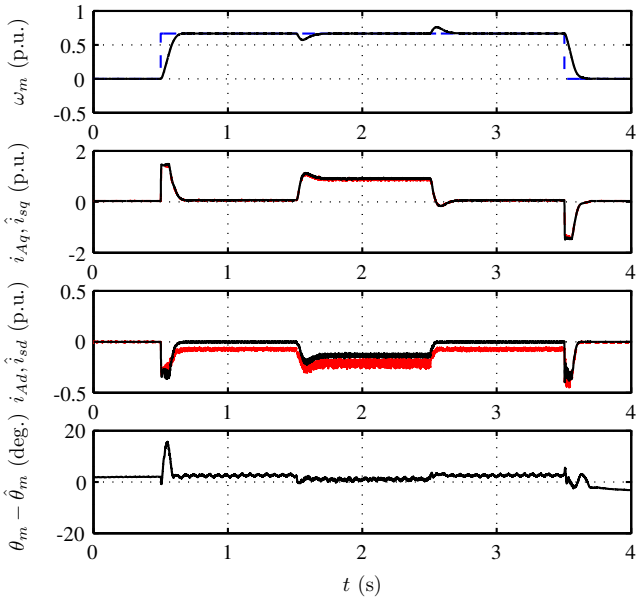

Fig. 8. Experimental results showing a sequence with speed and load changes. The first subplot shows the speed reference (dashed), the actual rotor speed (solid), and its estimate (dotted). The second subplot shows the q components of the estimated stator current (solid) and actual inverter current (dashed). The third subplot shows the d components of the estimated stator current (solid) and actual inverter current (dashed). The fourth subplot shows the estimation error of the rotor position in electrical degrees.

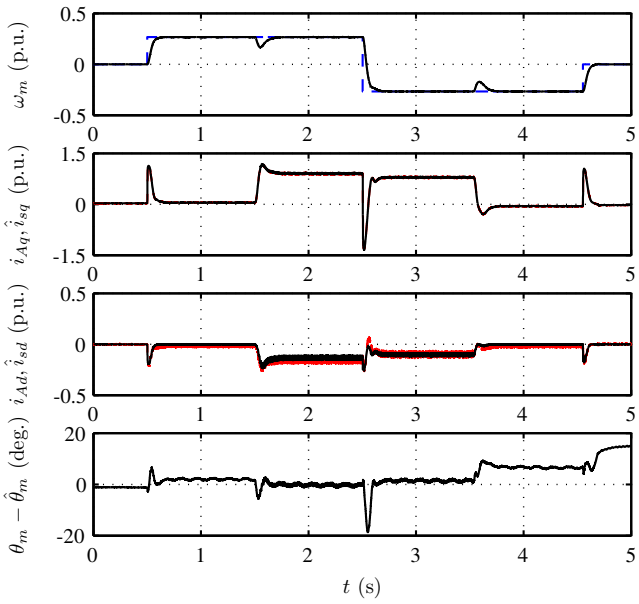

Fig. 9. Experimental results showing a sequence with speed and load changes. The explanations of the curves are as in Fig. 8.

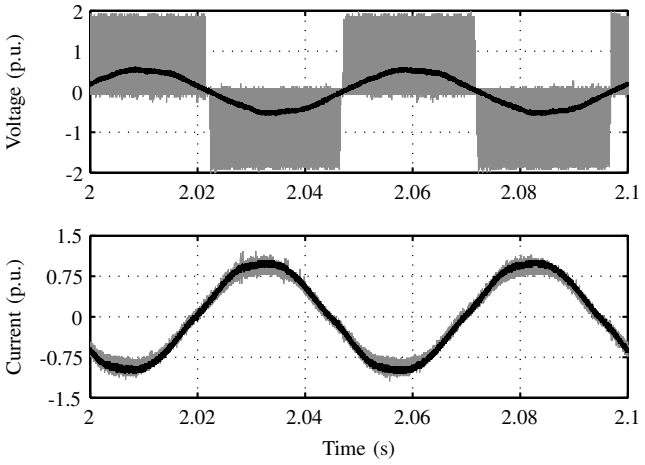

Fig. 10. Voltage and current waveforms from experiment in Fig. 9. The first subplot shows the inverter output voltage (phase-to-phase) and the stator voltage (phase-to-phase). The second subplot shows the inverter current and the stator current.

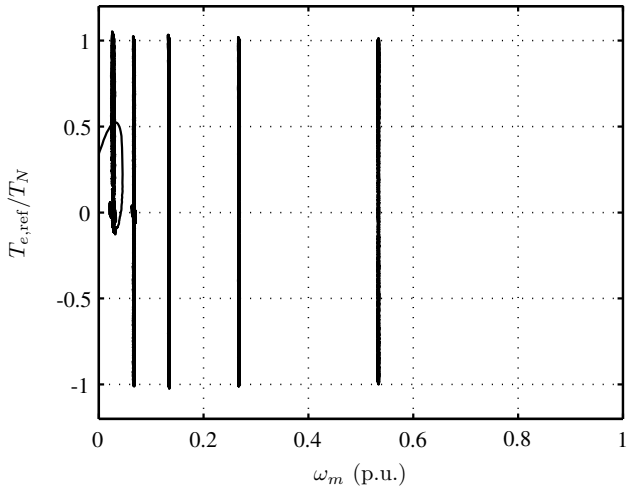

Fig. 11. Experimental results showing speed-torque curves as speed reference is kept constant and load torque is changed from rated torque T_N to $-T_N$.

ACKNOWLEDGMENT

The authors would like to thank ABB Oy, Walter Ahlström Foundation, and Tekniikan edistämissäätiö for the financial support.

REFERENCES

[1] Y. Murai, T. Kubota, and Y. Kawase, "Leakage current reduction for a high-frequency carrier inverter feeding an induction motor," *IEEE Trans. Ind. Applicat.*, vol. 28, no. 4, pp. 858–863, July/Aug. 1992.

[2] H. Akagi, H. Hasegawa, and T. Doumoto, "Design and performance of a passive EMI filter for use with a voltage-source PWM inverter having sinusoidal output voltage and zero common-mode voltage," *IEEE Trans. Power Electron.*, vol. 19, no. 4, pp. 1069–1076, July 2004.

[3] Y. Sozer, D. A. Torrey, and S. Reva, "New inverter output filter topology for PWM motor drives," *IEEE Trans. Power Electron.*, vol. 15, no. 6, pp. 1007–1017, Nov. 2000.

[4] M. Carpita, D. Colombo, A. Monti, and A. Fradilli, "Power converter filtering techniques design for very high speed drive systems," in *Proc. EPE'01*, Graz, Austria, Aug. 2001.

[5] T. D. Batzel and K. Y. Lee, "Electric propulsion with sensorless permanent magnet synchronous motor: implementation and performance," *IEEE Trans. Energy Conversion*, vol. 20, no. 3, pp. 575–583, Sep. 2005.

[6] J.-D. Park, C. Khalizadeh, and H. Hofmann, "Design and control of high-speed solid-rotor synchronous reluctance drive with three-phase LC filter," in *Conf. Rec. IEEE-IAS Annu. Meeting*, Hong Kong, China, Oct. 2005, pp. 715–722.

[7] W. Zimmermann, "Feldorientiert geregelter Umrichterantrieb mit sinusförmigen Maschinenspannungen," *etzArchiv*, vol. 10, no. 8, pp. 259–266, Aug. 1988.

[8] A. Nabae, H. Nakano, and Y. Okamura, "A novel control strategy of the inverter with sinusoidal voltage and current outputs," in *Proc. IEEE PESC'94*, vol. 1, Taipei, Taiwan, June 1994, pp. 154–159.

[9] H. Rapp and J. Haag, "Stator current control for high-speed induction machines operated from inverters with LC-output-filter," *European Transactions on Electrical Power*, vol. 7, no. 4, pp. 235–242, July/Aug. 1997.

[10] M. Petkovšek, P. Zajec, and J. Nastran, "Magnetizing rotor flux determination using a time-discrete voltage source inverter," in *Proc. MELECON 2000*, Nicosia, Cyprus, May. 2000.

[11] R. Seliga and W. Koczara, "Multiloop feedback control strategy in sine-wave voltage inverter for an adjustable speed cage induction motor drive system," in *Proc. EPE'01*, Graz, Austria, Aug. 2001, CD-ROM.

[12] M. Kojima, K. Hirabayashi, Y. Kawabata, E. C. Ejiogu, and T. Kawabata, "Novel vector control system using deadbeat-controlled PWM inverter with output LC filter," *IEEE Trans. Ind. Applicat.*, vol. 40, no. 1, pp. 162–169, Jan./Feb. 2004.

[13] J. Salomäki and J. Luomi, "Vector control of an induction motor fed by a PWM inverter with output LC filter," *EPE Journal*, vol. 16, no. 1, pp. 37–43, 2006.

[14] J. Salomäki, M. Hinkkanen, and J. Luomi, "Sensorless vector control of an induction motor fed by a PWM inverter through an output LC filter," *Trans. IEEJ*, vol. 126-D, no. 4, pp. 430–437, Apr. 2006.

[15] ——, "Sensorless control of induction motor drives equipped with inverter output filter," *IEEE Trans. Ind. Electron.*, vol. 53, no. 4, Aug. 2006, in press.

[16] L. Springob and J. Holtz, "High-bandwidth current control for torque-ripple compensation in PM synchronous machines," *IEEE Trans. Ind. Electron.*, vol. 45, no. 5, pp. 713–721, Oct. 1998.

[17] T. Jahns, G. Kliman, and T. Neumann, "Interior permanent-magnet synchronous motors for adjustable-speed drives," *IEEE Trans. Ind. Applicat.*, vol. 22, no. 4, pp. 738–747, July/Aug. 1986.

[18] J. Niiranen, "Fast and accurate symmetric Euler algorithm for electromechanical simulations," in *Proc. Electrimacs'99*, vol. 1, Lisboa, Portugal, Sept. 1999, pp. 71–78.

[19] C. Schauder, "Adaptive speed identification for vector control of induction motors without rotational transducers," *IEEE Trans. Ind. Applicat.*, vol. 28, no. 5, pp. 1054–1061, Sept./Oct. 1992.

[20] M. Hinkkanen, "Analysis and design of full-order flux observers for sensorless induction motors," *IEEE Trans. Ind. Electron.*, vol. 51, no. 5, pp. 1033–1040, Oct. 2004.

[21] A. Piippo, M. Hinkkanen, and J. Luomi, "Analysis of an adaptive observer for sensorless control of PMSM drives," in *Proc. IEEE IECON'05*, Raleigh, NC, Nov. 2005, pp. 1474–1479.

[22] J. K. Pedersen, F. Blaabjerg, J. W. Jensen, and P. Thøgersen, "An ideal PWM-VSI inverter with feedforward and feedback compensation," in *Proc. EPE'93*, vol. 4, Brighton, U.K., Sept. 1993, pp. 312–318.